Nanoscale

Accepted Manuscript

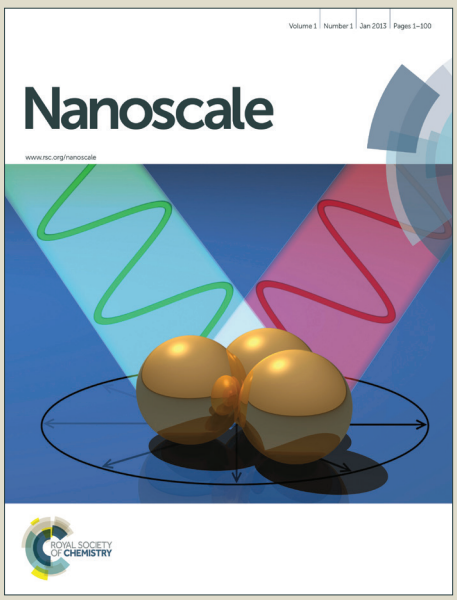

ROYAL SOCIETY OF CHEMISTRY

www.rsc.org/nanoscale

Cite this: DOI: 10.1039/c0xx00000x

www.rsc.org/xxxxxx

ARTICLE TYPE

A simple way to prepare Au@polypyrrole/Fe_3O_4 hollow capsules with high stability and their application in catalytic reduction of methylene blue dye

Tongjie Yao,[a] Tieyu Cui,*[a] Hao Wang,[a] Linxu Xu,[a] Fang Cui[a] and Jie Wu*[b]

Received (in XXX, XXX) Xth XXXXXXXXX 20XX, Accepted Xth XXXXXXXXX 20XX
DOI: 10.1039/b000000x

Metal nanoparticles are promising catalysts for dye degradation in treating wastewater despite the challenges of recycling and stability. In this study, we have introduced a simple way to prepare Au@polypyrrole (PPy)/Fe_3O_4 catalysts with Au nanoparticles embedded in PPy/Fe_3O_4 capsule shell. The PPy/Fe_3O_4 capsule shell used as support was constructed in one-step, which not only dramatically simplified the preparation process, but also made the magnetic property of catalysts can be easily controlled through adjusting the dosage of $FeCl_2 \cdot 4H_2O$. The component Au nanoparticles could catalyze the reduction of methylene blue dye with $NaBH_4$ as reducing agent, and the reaction rate constant was calculated through the pseudo-first-order reaction equation. The Fe_3O_4 nanoparticles permitted quick recycling of the catalysts with a magnet due to their room-temperature superparamagnetic property; therefore, the catalysts exhibited good reusability. In addition to catalytic activity and reusability, stability was also an important property for catalysts. Because both Au and Fe_3O_4 nanoparticles were wrapped in PPy shell, compared with precursor polystyrene/Au composites and bare Fe_3O_4 nanoparticles, the stability of Au@PPy/Fe_3O_4 hollow capsules was greatly enhanced. Since the current method was simple and flexible to create recyclable catalysts with high stability, it would promote the practicability of metal nanoparticle catalysts in industrial polluted water treatment.

Introduction

Metal nanoparticles have drawn more and more attention due to their fantastic physical, chemical and biological properties. These merits make them have wide applications in energy conversion, sensor, biomedicine, and especially in catalysis.[1-4] A number of studies have shown that metal nanoparticles exhibit unexpectedly high catalytic activities toward different types of reactions due to their high surface area-to-volume ratio. However, there are two drawbacks that greatly hinder their applications in real life: first, the aggregation of metal nanoparticles in solution results in remarkable reduction in their catalytic activities; second, they are difficult to be recycled from reaction solution due to small size. During the past two decades, many attempts have been done to overcome these drawbacks. It has been proven through investigations that anchoring metal nanoparticles on supports is an effective approach to solve the above two drawbacks.[5-7] Therefore, many materials with active sites for anchoring metal nanoparticles have been developed as candidates for catalyst supports. Of wide range of supports, hollow capsules have attracted considerable interest due to their low density, high surface area and large void volume.[8-10] There are three different positions for hollow capsules to load metal nanoparticles: on the surface, inside of capsule and embedded in the shell.[11-13] Once the metal nanoparticles are anchored on the support surface, they directly expose to the reaction solutions, which may cause them fall off from the support and deactivate by solution erosion. When metal nanoparticles are loaded inside of hollow capsules, the major problem they faced is still the aggregations after long-time use. Compared with above two positions, it is more appreciable to embed metal nanoparticles in the capsule shell, which can effectively hinder them fall off and aggregate through the protection of capsule shell; and hence, the stability of metal nanoparticles is improved.

Besides good catalytic activity and high stability, recycling is another important property for catalysts. It is well known to us, the traditional separation techniques, such as centrifugation and filtration, are usually time-consuming and low efficiency, which was not favored for recycling of catalysts.[14] Compared with traditional separation techniques, magnetic separation has distinct advantage. Combining magnetic nanoparticles with hollow capsule supports not only enables the catalysts to have the magnetic separation property, but also facilitates them to be quickly recycled. Because of these advantages, many research groups have devoted their effort to prepare magnetic hollow

[a]*The Academy of Fundamental and Interdisciplinary Science, Harbin Institute of Technology, Harbin, Heilongjiang 150080, People's Republic of China; E-mail: cuit@hit.edu.cn*
[b]*School of Chemistry and Materials Science, Heilongjiang University, Harbin 150080, People's Republic of China; E-mail: wujieeasy@163.com*

capsules as supports to load metal nanoparticles.[15-17] However, the main obstacle to construct such supports is that the preparation procedure is generally very complex and comprises multi-step treatments.[18-20] Therefore, design and synthesis of catalysts with good catalytic activity and high stability, together with magnetic property, in a simple way is still highly desirable.

In this paper, we have designed a simple way to fabricate Au@polypyrrole (PPy)/Fe_3O_4 hollow capsules with the high stability and good catalytic property. In our method, Au nanoparticles were embedded in the PPy/Fe_3O_4 capsule shell. Due to the coverage and isolation of the PPy chain, the Au nanoparticles could hardly escape from the capsule shell or contact with each other, thus avoiding falling off and aggregation. In addition, compared with traditional procedure,[21,22] the PPy/Fe_3O_4 capsule shell was synthesized in one-step, which not only simplified the preparation procedure, but also made the magnetic property of catalysts could be easily controlled. The catalytic property of Au@PPy/Fe_3O_4 hollow capsules was investigated by reducing the methylene blue (MB) dye with $NaBH_4$ as the reducing agent. Owing to the incorporation of Fe_3O_4 nanoparticles, the catalysts could be easily separated from reaction solution by an external magnetic field and reused. More significantly, the stability of Au@PPy/Fe_3O_4 hollow capsules was addressed in detail.

Experimental methods

Materials

The pyrrole monomer was purchased from Sigma–Aldrich, and it was distilled under reduced pressure and stored at -4 ^oC prior to use. Styrene, acrylic acid, methylacrylic acid, sodium citrate, absolute ethanol, poly(diallyldimethylammonium chloride) (PDDA), tetrahydrofuran (THF), methylene blue (MB) dye, $NH_3 \cdot H_2O$ (28 wt%), $K_2S_2O_8$, $FeCl_3 \cdot 6H_2O$, $FeCl_2 \cdot 4H_2O$, $HAuCl_4$ and $NaBH_4$ were purchased from Sinopharm Chemical Reagent Co., Ltd. All of chemicals were analytical grade and used as received. The water used in the experiments was deionized with a resistivity of 18.2 $M\Omega \cdot cm^{-1}$.

Synthesis of Au nanoparticles

Firstly, the mixture of 500 μL $HAuCl_4$ (100 mM) and 200 mL deionized water was heated to boiling under magnetic stirring. Then, 5 mL sodium citrate aqueous solution (2 wt%) was added into above mixture. The solution color gradually changed from light yellow to purple and finally be red. When the solution color reached red, the solution was naturally cooled down to room temperature, and the Au nanoparticles with average diameter of 10 nm were obtained. The concentration of as-prepared Au nanoparticles was about 1.5 mg/mL.

Synthesis of PS/Au composites

Carboxylic-capped polystyrene (PS) nanospheres were prepared according to the previous reports.[23,24] To prepare PS/Au composites, first, the carboxylic-capped PS nanospheres (55 mg) were mixed with 20 mL PDDA aqueous solution (5 wt%) and stirred for 2.0 h. Then, the excess PDDA was removed by three cycles of centrifugation and washing with deionized water. Subsequently, the PDDA-modified PS nanospheres were added into the 80 mL as-prepared Au nanoparticle solution under magnetic stirring. After 0.5 h, the mixture was centrifuged and washed by water to remove isolated Au nanoparticles. Finally, the obtained PS/Au composites were re-dispersed into 30 mL water for next-step.

Preparation of Au@PPy/Fe_3O_4 hollow capsules

In a typical synthesis, 50 μL pyrrole monomer was injected into the above PS/Au composite solution under mechanical stirring at ambient temperature. 0.5 h later, 3.0 mL $FeCl_3 \cdot 6H_2O$ solution (5 wt%) was added into the mixture slowly. The oxidation polymerization was maintained for 5.0 h before nitrogen was purged into solution to remove oxygen. Then, 50 mg $FeCl_2 \cdot 4H_2O$ and 1.0 mL $NH_3 \cdot H_2O$ were added into system successively. The reaction was allowed to proceed for another 3.0 h under nitrogen protection, and the PS/Au@PPy/Fe_3O_4 composites were prepared. Finally, to obtain Au@PPy/Fe_3O_4 hollow capsules, the as-prepared PS/Au@PPy/Fe_3O_4 composites were suspended into 30 mL THF solution. After stirring for a night, the PS nanospheres were removed, and the resulting Au@PPy/Fe_3O_4 hollow capsules were separated by magnet and washed by ethanol.

Catalyzed reduction of MB dye

The catalytic property of Au@PPy/Fe_3O_4 hollow capsules was explored by studying the change of the absorbance intensity at the maximum absorbance wavelength (λ_{max}) of the MB dye. In a typical procedure, 2.0 mg Au@PPy/Fe_3O_4 hollow capsules were homogeneously dispersed into the 2.5 mL MB dye solution (24 mg/L), followed by a rapid injection of 1.0 mL of $NaBH_4$ solution (15 mg/mL). The color of the mixture gradually changed from blue to colorless, indicating the Au@PPy/Fe_3O_4 hollow capsules catalyzed the reduction of the MB dye. In the recycling study, the catalysts were separated from the solution by magnet when the reduction reaction completely finished. After washed by water twice, they were reused in the next reaction run. The procedure was repeated for 5 times. After reaction with 2.0 mg catalysts for 20 min in each cycle, the absorbance intensity of reaction solution was immediately measured and the conversation of MB dye was calculated.

Characterization

A JEOL JSM-6700F scanning electron microscope (SEM) with primary electron energy of 3 kV was employed to examine the surface morphologies of products. The structure and shell thickness of the materials, crystalline lattice of nanoparticles, energy dispersive absorption X-ray (EDX) spectrum and element mappings were determined by Tecnai G^2 F30, transmission electron microscope (TEM) operating at 300 kV. Fourier-transform infrared (FT-IR) spectra were measured in wavenumber ranging from 400 to 4000 cm^{-1} using Nicolet Avatar 360 FT-IR spectrophotometer. Lambda 750 ultraviolet and visible (UV-Vis) spectrophotometer was employed for analysis of MB dye reduction. X-ray diffraction (XRD) data was collected on a Siemens D-5005 X-ray diffractometer with Cu Kα radiation (λ = 1.5418 Å). The Field-Magnetization dependence of the products was measured using a MPMS-7 superconducting quantum interference device (SQUID) magnetometer at magnetic fields up to 50 kOe. Inductively coupled plasma atomic spectrum (ICP) was performed on Optima 7000 DV. The zeta-potential was

measured using a Horiba SZ-100 zeta-potential analyzer, the samples were diluted and the pH value was set around 7.0 before analysis. X-ray photoelectron spectroscopy (XPS) was collected by using a VG ESCALAB MKII spectrometer with Mg Kα excitation (1253.6 eV). Binding energy calibration was based on C 1s at 284.6 eV.

Results and Discussion

Fig. 1 outlines the overall procedure, which begins with preparation of PS/Au composites by adsorbing negatively charged Au nanoparticles on the surface of PDDA modified PS nanoparticles. Then, $FeCl_3 \cdot 6H_2O$ was added into mixture of PS/Au composites and pyrrole monomer to initiate polymerization of pyrrole monomer. When the reaction proceeded, $FeCl_2 \cdot 4H_2O$ and $NH_3 \cdot H_2O$ were added into the system successively under nitrogen protection. In alkaline condition, Fe_3O_4 nanoparticles were synthesized and wrapped into the PPy shell, and the PS/Au@PPy/Fe_3O_4 composites were prepared. Finally, to obtain Au@PPy/Fe_3O_4 hollow capsules, the as-prepared PS/Au@PPy/Fe_3O_4 composites were soaked in THF solution for a night to remove PS cores.

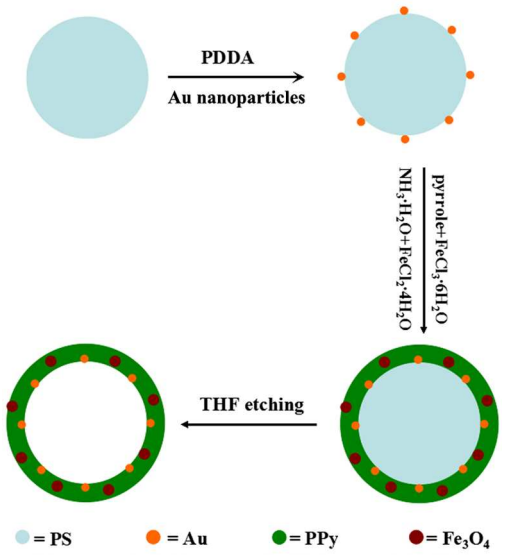

Fig. 1 Schematic illustration of the preparation procedure of Au@PPy/Fe_3O_4 hollow capsules.

In our study, monodispersed PS nanospheres were used as the hard-templates to load Au nanoparticles and constructed resulting hollow capsules. Fig. 2a shows the SEM image of PS nanospheres. They have a uniform spherical shape with diameter around of 400 nm. From the magnified image, we can see their surface is very smooth (inset of Fig. 2a). A zeta-potential of -83.2 mV indicated that the PS nanospheres had large numbers of negative charges on their surfaces in water. As commonly known, Au nanoparticles whose surface was stabilized by sodium citrate exhibited negative charge and their zeta-potential value was -38.0 mV. Therefore, to adsorb Au nanoparticles on the surface of PS nanospheres, cationic PDDA had to be first adsorbed on PS nanosphere surface to produce PDDA modified PS nanospheres with a zeta-potential of +33.0 mV. After PDDA modification, the obtained PS nanospheres with positively charged surface made them favorable for electrostatic attachment with negatively charged Au nanoparticles. As observed in Fig. 2b, the Au nanoparticles with average diameter of 10 nm are decorated on the PS nanosphere surface, which leads to a raspberry-like morphology of PS/Au composites.

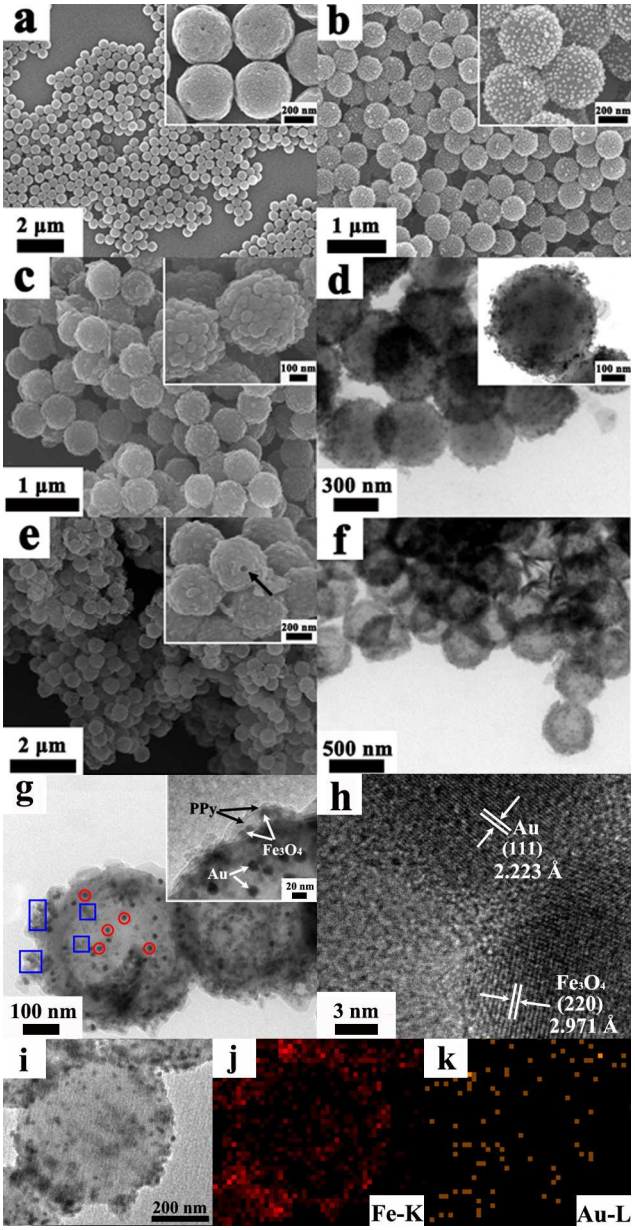

Fig. 2 (a) SEM image of PS nanospheres; (b) SEM image of PS/Au composites; (c) SEM image of PS/Au@PPy/Fe_3O_4 composites; (d) TEM image of PS/Au@PPy/Fe_3O_4 composites; (e) SEM image of Au@PPy/Fe_3O_4 hollow capsules; (f) TEM image of Au@PPy/Fe_3O_4 hollow capsules; (g) TEM image of Au@PPy/Fe_3O_4 hollow capsules at higher magnification, the Au nanoparticles are pointed by red cycle and Fe_3O_4 nanoparticles are pointed by blue boxes; (h) high-resolution TEM image of Au and Fe_3O_4 nanoparticles embedded in PPy shell. The insets show the corresponding magnified images. (i~k) TEM image and corresponding element mappings of Au@PPy/Fe_3O_4 hollow capsules.

When the oxidant $FeCl_3 \cdot 6H_2O$ was added into the mixture of pyrrole monomer and PS/Au composites, the color of the solution gradually changed from light purple to black, indicating the oxidation polymerization of pyrrole monomer took place. When

polymerization was proceeding, $FeCl_2 \cdot 4H_2O$ and $NH_3 \cdot H_2O$ were added successively into the reaction system under nitrogen protection. Introduction of $NH_3 \cdot H_2O$ into the reaction system quickly increased the alkalinity of mixture, which resulted in the hydrolysis of both $FeCl_3 \cdot 6H_2O$ and $FeCl_2 \cdot 4H_2O$. Therefore, $Fe(OH)_3$ and $Fe(OH)_2$ were produced under alkaline condition, and finally Fe_3O_4 nanoparticles formed through dehydration. In experiment, $FeCl_3 \cdot 6H_2O$ played two roles: first, they acted as the oxidant to initiate polymerization of pyrrole monomer; second, they used as the source of resulting Fe_3O_4 nanoparticles. The morphology of PS/Au@PPy/Fe_3O_4 composites is exhibited in Fig. 2c. As an obvious comparison between Fig. 2a and Fig. 2c, the PS/Au@PPy/Fe_3O_4 composites show a considerable rough surface and this is the feature of PPy homopolymer.[25,26] Their rough surface can also be observed better in a magnified SEM image (inset of Fig. 2c). In addition to the difference in morphology, compared with original PS/Au composites, the diameter of PS/Au@PPy/Fe_3O_4 composites increased from 400 to 500 nm, which further suggested a successful coating of the PPy/Fe_3O_4 shell around the PS/Au composite surface, and their shell thickness was calculated to be 50 nm. Fig. 2d shows the corresponding TEM image of PS/Au@PPy/Fe_3O_4 composites. It is difficult to resolve the interface between PPy shell and PS core due to their similar electron contrast, and only solid composites with spherical morphology can be seen. However, in magnified TEM image (inset of Fig. 2d), it is easy to distinguish that many inorganic nanoparticles randomly decorate in the PPy shell.

To obtain Au@PPy/Fe_3O_4 hollow capsules, THF solution was selected to etch the PS core in PS/Au@PPy/Fe_3O_4 composites. Fig. 2e shows the SEM image of Au@PPy/Fe_3O_4 hollow capsules. They have the similar rough morphology as PS/Au@PPy/Fe_3O_4 composites, indicating the PPy/Fe_3O_4 shell was well preserved during the THF etching process. The inner hollow structure is clearly observed from the ruptured capsules as pointed out by arrow in inset of Fig. 2e, which can be further evidenced by TEM image. The TEM image in Fig. 2f confirms that the Au@PPy/Fe_3O_4 capsules possess a well-defined hollow structure, as a large void appears owing to the removal of PS core. The PPy/Fe_3O_4 shell thickness is measured to be 50 nm, which is in a good agreement with the value calculated from the SEM image.

Besides hollow structure, another obvious phenomenon in magnified image of Au@PPy/Fe_3O_4 hollow capsules is that many inorganic nanoparticles decorate in the capsule shell (Fig. 2g). As Au nanoparticles scattered more electrons, they looked much darker than Fe_3O_4 nanoparticles. In addition, the morphology of Fe_3O_4 nanoparticles was not as uniform as Au nanoparticles. According to above difference, it could be easily distinguished Au nanoparticles from Fe_3O_4 nanoparticles. In Fig. 2g, we have pointed Au nanoparticles by red circles and Fe_3O_4 nanoparticles by blue boxes. The size of Fe_3O_4 nanoparticles is measured to be 23.7 nm, which is lager than the diameter of Au nanoparticles. In the high-resolution TEM image (Fig. 2h), the crystalline lattice of both Au and Fe_3O_4 nanoparticles can be well observed. The distance between two adjacent lattice planes is approximately 2.223 and 2.971 Å, which corresponds to (111) and (220) lattice of Au and Fe_3O_4 nanoparticles, respectively. To better observe the distribution of Au and Fe_3O_4 nanoparticles in hollow capsules, the element mappings of Fe and Au were shown in Fig. i~k. Although some isolated Fe_3O_4 nanoparticles decorate on the hollow capsule surface, most Fe_3O_4 nanoparticles uniformly embed in the capsule shell, while the Au nanoparticles randomly distribute. EDX analysis (Fig. S1) indicate the weight ratio of Fe_3O_4 to Au nanoparticles in hollow capsules is about 8.5. Since PPy layer directly wrapped around PS/Au composite surface, Au nanoparticles were embedded in the capsule shell, which made Au nanoparticles hardly escape from the capsules. Moreover, since the PPy chain isolated Au nanoparticles from each other during polymerization, no aggregation of Au nanoparticles could be seen in TEM image. These two aspects were favorable for preserving catalytic property of Au nanoparticles. In our study, when Fe_3O_4 nanoparticles start to form, the polymerization of pyrrole monomer still proceed; therefore, similar to Au nanoparticles, most Fe_3O_4 nanoparticles are wrapped in PPy shell (inset of Fig. 2g). This was very important for improving their stability and we would discuss it later.

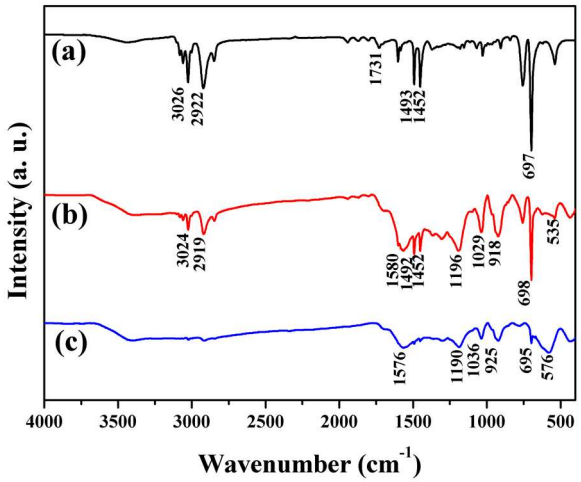

Fig. 3 FT-IR spectra of (a) PS/Au composites; (b) PS/Au@PPy/Fe_3O_4 composites; (c) Au@PPy/Fe_3O_4 hollow capsules;

Fig. 3 shows the FT-IR spectra of PS nanospheres, PS/Au@PPy/Fe_3O_4 composites and Au@PPy/Fe_3O_4 hollow capsules. In Fig. 3a, the PS main peaks locate at 3026, 2922, 1493, 1452 and 697 cm^{-1}. In addition, a peak appears at 1731 cm^{-1}, suggesting carboxylic group is successfully modified on their surface. After PPy/Fe_3O_4 shell was coated on the surface of PS/Au composites, the PS/Au@PPy/Fe_3O_4 composites were prepared. In spectrum (Fig. 3b), the main peaks of PS nanospheres appear at 3024, 2919, 1492, 1452 and 698 cm^{-1}. The characteristic band at 1580 cm^{-1} is attributed to the stretching mode of the C–C in the pyrrole ring, and ring deformation at 918 cm^{-1} is also observed. The peak at 1196 cm^{-1} is related to the in-plane vibrations of C–H. The band at 1029 cm^{-1} is assigned to the C–H in-plane bending mode.[27] Moreover, the band at 535 cm^{-1} is corresponding to the stretching mode of Fe–O in Fe_3O_4 nanoparticles.[28] FT-IR spectrum, together with SEM and TEM images, indicated that PS/Au@PPy/Fe_3O_4 composites had been successfully prepared. Fig. 3c shows the FT-IR spectrum of Au@PPy/Fe_3O_4 hollow capsules. The peaks located at 1576, 1190, 1036 and 925 cm^{-1} belong to the PPy chain. A weak peak appeared at 695 cm^{-1} reveals that although PS cores vanish in the view of TEM image, the trace amounts of PS chains still remain

in Au@PPy/Fe_3O_4 hollow capsules.[29] This might be because a number of pores in PPy shell were blocked by Au and Fe_3O_4 nanoparticles during the preparation, which greatly increased the difficulty for dissolved PS chains completely diffusing out of the capsule shell.

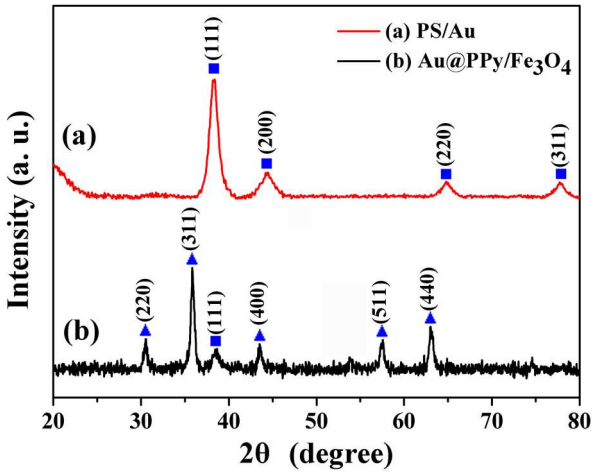

Fig. 4 XRD pattern of (a) PS/Au composites; (b) Au@PPy/Fe_3O_4 hollow capsules; ■represents Au nanoparticles; ▲represents Fe_3O_4 nanoparticles.

Fig. 4a shows the wide angle XRD pattern of PS/Au composites. Four diffraction peaks appear at 2θ = 38.2, 44.6, 64.8 and 77.7°, which are corresponding to (111), (200), (220) and (311) Bragg reflections of cubic lattice of Au nanoparticles (JCPDS No. 04-0784), respectively.[30] Fig. 4b is corresponding to the XRD pattern of Au@PPy/Fe_3O_4 capsules, five diffraction peaks appear at 2θ = 30.6, 35.8, 43.4, 57.5 and 63.2°, which are corresponding to (220), (311), (400), (511) and (440) Bragg diffractions of the cubic lattice of Fe_3O_4 nanoparticles (JCPDS no. 19-0629), respectively.[31] As commonly known, it was hard to distinguish Fe_3O_4 and γ-Fe_2O_3 from XRD pattern due to their similarity. Therefore, XPS measurement is carried out to determine that the samples are Fe_3O_4 nanoparticles (Fig. S2). According to previous report,[32,33] although the binding energies of Fe_3O_4 and γ-Fe_2O_3 were very close; however, once γ-Fe_2O_3 nanoparticles existed in samples, a peak centered at 719 eV could be observed. No apparent peak located at 719 eV can be found in our XPS spectrum; therefore, the magnetic nanoparticles in our hollow capsules are assigned as Fe_3O_4 nanoparticles. Using the Debye-Scherrer equation, the average diameter of Fe_3O_4 nanoparticles is estimated to be 21.2 nm, which is in a good agreement with the results measured from TEM image. In Fig. 4b, because of low weight content in hollow capsules, the diffraction peaks of Au nanoparticles nearly disappear except (111) Bragg reflection centered at 38.1°. ICP measurements showed the loading of Au nanoparticles in hollow capsules was around 4.6 wt%; while the weight percentage of Fe_3O_4 nanoparticles was as high as 41.4 wt%. The weight ratio of Fe_3O_4 to Au nanoparticles calculated by ICP measurements (9.0) was quite close to the value obtained from EDX spectrum (8.5).

In our study, PPy/Fe_3O_4 shell was prepared in one-step, which dramatically simplified the preparation process. In addition, we could control the magnetic property of Au@PPy/Fe_3O_4 hollow capsules through adjusted the dosage of $FeCl_2{\cdot}4H_2O$. When the usage of $FeCl_2{\cdot}4H_2O$ is 10, 30 and 50 mg, the loading of Fe_3O_4 nanoparticles in hollow capsules was 36.2, 40.1 and 41.4 wt%, respectively. Although the dosage of $FeCl_2{\cdot}4H_2O$ had little influence on Fe_3O_4 nanoparticles loading due to their low usage, they had great effect on the magnetic properties of Au@PPy/Fe_3O_4 hollow capsules. Fig. 5 shows the magnetization curves of the Au@PPy/Fe_3O_4 hollow capsules with different dosage of $FeCl_2{\cdot}4H_2O$. When the dosage of $FeCl_2{\cdot}4H_2O$ is 10, 30 and 50 mg, the magnetization value of Au@PPy/Fe_3O_4 hollow capsules is 27.3, 34.7 and 38.5 emu/g, respectively, indicating $FeCl_2{\cdot}4H_2O$ contributes to the magnetic property of Au@PPy/Fe_3O_4 hollow capsules. The nearly zero coercivity and the reversible hysteresis behavior indicate the room-temperature superparamagnetic nature of the catalysts. In addition, the hysteresis loops at 5 K are also measured (Fig. S3), the Au@PPy/Fe_3O_4 hollow capsules are ferromagnetic at low temperature, suggesting the diameter of obtained Fe_3O_4 is larger than their critical size.[34,35] A question was presented: why the weight percentages of Fe_3O_4 nanoparticles in three samples were close, but their magnetization increased with the dosage of $FeCl_2{\cdot}4H_2O$? We thought that not all Fe_3O_4 nanoparticles did their contribution to the magnetization of products. Although some Fe^{3+} and Fe^{2+} ions formed Fe_3O_4 nanoparticles with diameter larger than critical size. Other Fe^{3+} ions, together with Fe^{2+} ions originated from reduction of Fe^{3+} ions, diffused into the interspace of the PPy chain during the polymerization.[36] When $NH_3{\cdot}H_2O$ was added, these ions reacted with $NH_3{\cdot}H_2O$ to form hydroxide, and finally be oxide nanoparticles through dehydration. As the size of these oxide nanoparticles inside of the PPy chain was too small to form ordered crystal structure, no peaks belonged to them were observed in XRD pattern, and they also had little contribution to magnetization. However, in ICP measurements, they could be dissolved by aqua regia, and contributed to the concentration of element Fe. When the usage of $FeCl_2{\cdot}4H_2O$ increased, more and more Fe_3O_4 nanoparticles with diameter larger than critical size synthesized. Therefore, the magnetization intensity increased with the usage of $FeCl_2{\cdot}4H_2O$.

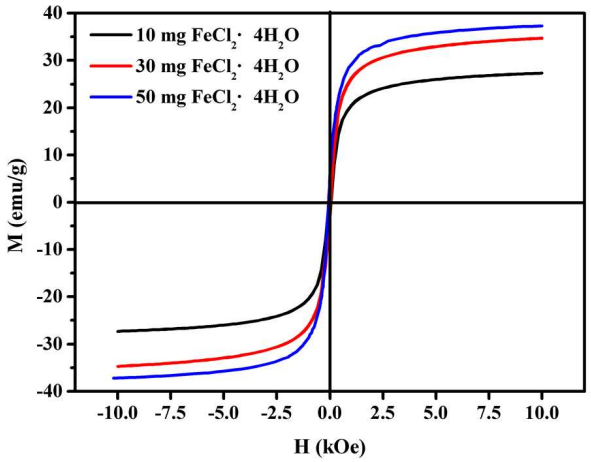

Fig. 5 Magnetization curves at 295 K of Au@PPy/Fe_3O_4 hollow capsules with different amount of $FeCl_2{\cdot}4H_2O$, while other parameters were the same.

It has been experimentally demonstrated that Au nanoparticles have high catalytic activity in carbon–carbon coupling reaction, hydrogenation, and reduction of various dyes.[37-39] Inspired by these ideas, here, we investigated the

application of Au@PPy/Fe_3O_4 hollow capsules in water treatment. MB dye, as a typical industrial pollutant, was selected as a model to examine the catalytic performance of the Au@PPy/Fe_3O_4 hollow capsules with $NaBH_4$ as reducing agents under ambient conditions. Because the dark blue color of solution gradually vanished, the results of the reduction reaction could be roughly monitored through the naked eyes. Fig. 6a illustrates the UV–Vis spectra of the MB dye during the reaction in the presence or absence of the Au@PPy/Fe_3O_4 hollow capsules. Curve (a) is the UV–Vis spectrum of the initial MB dye solution with the color of dark blue and the λ_{max} appears at 664 nm (inset of Fig. 6a). As commonly known, amorphous PPy was good adsorbents for various dyes. Therefore, before studying catalytic activity, we had to investigate the adsorption of MB dyes in the presence of Au@PPy/Fe_3O_4 hollow capsules. Curve (b) shows the UV-Vis spectrum of MB dye solution after adding catalysts for 1.0 h, as only 7.2 % concentration decrease was observed, indicating that the adsorption was not the critical factor for reduction of initial MB dye solution concentration. Curve (c) is the corresponding UV–Vis spectrum of the mixture containing MB dye and $NaBH_4$ solution reacting for 25 h. The absorbance intensity at λ_{max} of MB decreases 91.7 %, but does not completely vanish. The color of the mixture becomes light blue (inset of Fig. 6a). When a trace amount of the Au@PPy/Fe_3O_4 hollow capsules (2.0 mg) was introduced into the solution, the absorption peak at 664 nm vanished within 20 min. The solution color quickly changed from dark blue to colorless (inset of Fig. 6a). Based on the above UV–Vis analysis, it could be concluded that the Au@PPy/Fe_3O_4 hollow capsules had excellent catalytic performance.[40]

The reaction rate of MB dye reduction in the presence of $NaBH_4$ solution with the help of 2.0 mg Au@PPy/Fe_3O_4 hollow capsules was too quick to be monitored. Therefore, we had to reduce the amount of catalysts to 0.1 mg. Fig. 6b presents the UV-Vis spectra monitoring the reduction reaction of MB dye, measured at different times using Au@PPy/Fe_3O_4 hollow capsules as catalysts. At initial 18 min, the intensity of λ_{max} only slightly reduced. As commonly known, the reduction reaction between MB dye and $NaBH_4$ was catalyzed on the surface of Au nanoparticles. In Au@PPy/Fe_3O_4 hollow capsules, Au nanoparticles were wrapped deeply in capsule shell, which increased the difficulty for both MB dye and $NaBH_4$ contacting with Au nanoparticle surface, as they had to diffuse through the PPy/Fe_3O_4 shell. This phenomenon further implied that PPy/Fe_3O_4 shell could effectively hinder the reaction solution to directly contact with Au nanoparticles. After 18 min, the intensity of λ_{max} gradually decreases until the reaction completes at 42 min. Considering the reductant was highly excessive, this ensured the $NaBH_4$ concentration remained essentially constant during the reaction, which allowed the reduction could be considered as a pseudo-first-order reaction with regard to MB dye only.[41] The rate constant k was determined by a linear plot of $\ln(C_t/C_0)$ and reaction time t (the ratio of C_t to C_0, where C_t and C_0 were the MB dye concentrations at time t and 0, respectively, was measured from the relative intensity of the respective absorbance A_t/A_0). Inset of Fig. 6b shows the linear relationship between ln (C_t/C_0) and reaction time t in reduction reactions catalyzed by Au@PPy/Fe_3O_4 hollow capsules. As all these plots matched the pseudo-first-order reaction kinetics very well, the rate constant k could be calculated from the rate equation and the values was 0.266 min^{-1}. The rate constant of precursor PS/Au composites with the same Au loading as Au@PPy/Fe_3O_4 hollow capsules is also studied. Their value is measured to be 1.50 min^{-1} (Fig. S4), which is about 5.6 times higher than that of Au@PPy/Fe_3O_4 hollow capsules. This was mainly because Au nanoparticles on PS nanosphere surface directly exposed to the reaction solution, which dramatically accelerated the reaction rate. In comparison, Au nanoparticles embedded in PPy/Fe_3O_4 shell led to poor reactant contacting; therefore, the reaction rate constant of Au@PPy/Fe_3O_4 hollow capsules reduced. However, 0.266 min^{-1} was still an acceptable rate constant for reduction reaction of MB dye by $NaBH_4$ solution, as their rate constant was 3.68×10^{-2} h^{-1} in absence of catalysts (Fig. S5).

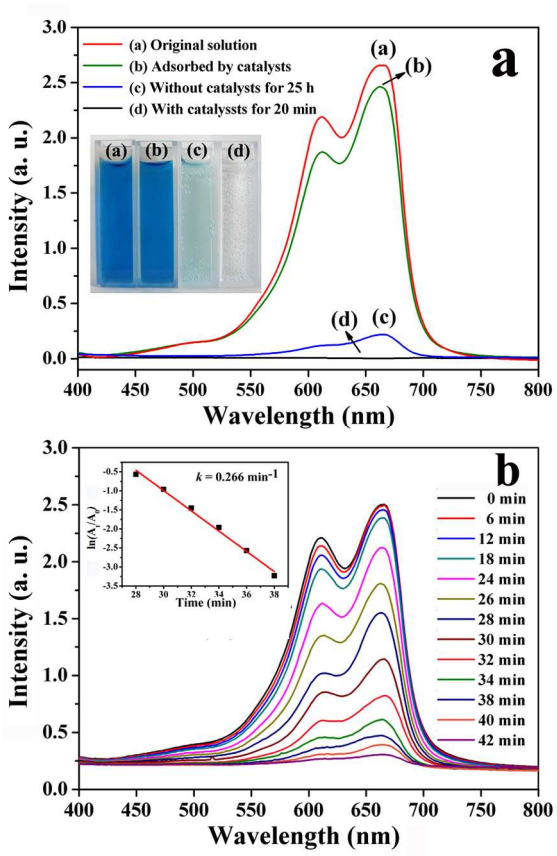

Fig. 6 (a) UV-Vis spectra of the original MB dye solution, MB dye solution after adsorption by catalysts for 1.0 h, mixture of MB dye and $NaBH_4$ solution after reaction for 25 h in the absence of catalysts, mixture of MB dye and $NaBH_4$ solution after reaction for 20 min in the presence of 2.0 mg Au@PPy/Fe_3O_4 hollow capsules; inset shows the corresponding digital camera photo. (b) UV-Vis spectra of the MB dye and $NaBH_4$ mixture in the presence of 0.1 mg Au@PPy/Fe_3O_4 catalysts at different times. Inset shows the rate constant k estimated by the slopes of straight lines of $\ln(A_t/A_0)$ vs. reduction time.

In addition to catalytic activity, stability was another important property for catalysts as it determined their service-life. According to the previous reports,[42,43] we have done the cycling test to study the reusability of Au@PPy/Fe_3O_4 hollow capsules. They could be easily collected from reaction solution by using a magnet and used for the next reaction due to their magnetic property (inset of Fig. 7a). Here, we repeat the separation–reuse

cycles 5 times. After reaction with 2.0 mg catalysts for 20 min in each cycles, the absorbance intensity of reaction solution was immediately measured by UV-Vis spectrum and the conversation of MB dye was calculated. As shown in Fig. 7a, even after five cycles, the conversion of MB dye is still nearly 100 %. To further studied their reusability, the reaction rate constant of each cycle is measured, and their value is 0.266, 0.249, 0.220, 0.206 and 0.151 min^{-1}, respectively (Fig. 7b and Fig. S6). As commonly known, although the catalysts could be easily recycled by magnet, their loss could not be avoided during the procedure of separation and rinsing. As the mass of catalysts was very little in this study (0.1 mg), any loss would affect catalytic activity. Therefore, the rate constant in each cycle gradually reduced. Besides studying the catalytic property of Au@PPy/Fe_3O_4 hollow capsules by the cycling test, we also investigate their integrity after 5 successive cycles by using SEM and TEM measurements (Fig. 7c and 7d). Compared with the initial materials (Fig. 2e-2g), there is no obvious difference in morphology, structure, and especially high dispersity of Au nanopartilces, which further confirms the good stability of Au@PPy/Fe_3O_4 hollow capsules.

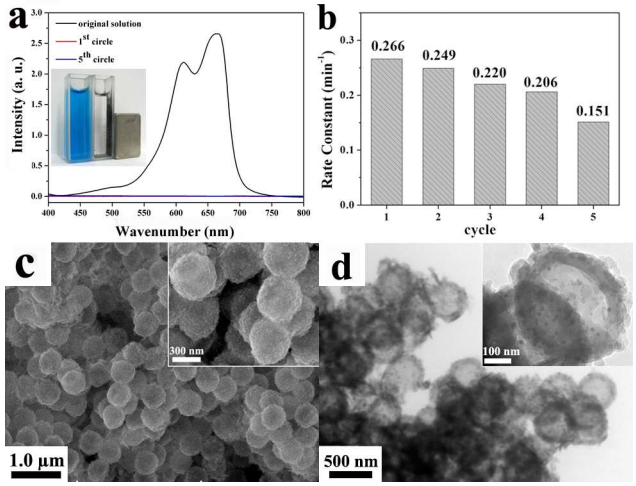

Fig. 7 (a) UV-Vis spectra of MB dye solution reduction with Au@PPy/Fe_3O_4 catalysts in different cycles; inset shows the corresponding digital camera photo took after 5th cycle. (b) the rate constant of each cycle. (c) SEM image of Au@PPy/Fe_3O_4 hollow capsules after used in catalytic tests for 5 times. The inset shows the magnified image; (d) TEM image of Au@PPy/Fe_3O_4 hollow capsules after used in catalytic tests for 5 times, the inset shows the magnified image.

As we known, it is hard to fully address the stability of catalysts through cycling tests due to the limits of cycling number. Earlier in this study, we have analyzed that compared with metal nanoparticles anchored on the support surface, metal nanoparticles embedded in the capsule shell would possess better stability, as the metal nanoparticles was more difficult to escape to exterior and be corroded by solution. Here, we compared the stability between Au@PPy/Fe_3O_4 hollow capsules and their precursor PS/Au composites through ultrasonic treatment and aqua regia etching test. First, Au@PPy/Fe_3O_4 hollow capsules and their precursor PS/Au composites with the same mass were placed in an ultrasound cleaner for 2.0 h in aqueous solution. After removing the catalysts, the mass of Au nanoparticles escaped from the PPy/Fe_3O_4 capsule shell or fall off from the PS nanoparticle surface was tested. ICP measurements showed that the loss of Au nanoparticles in Au@PPy/Fe_3O_4 hollow capsules was under the detection line of the instrument. In contrast, for PS/Au composites, Au nanoparticles with weight content of 1.39 wt% fall off from the PS nanosphere surface during the ultrasonic treatment. Next, in another control experiment, bare Fe_3O_4 nanoparticles, PS/Au composites and Au@PPy/Fe_3O_4 hollow capsules were added into the identical aqua regia solution with the concentration of 1.0 M. Au nanoparticles on the PS support surface were completely dissolved within 10 min. However, even extend the etching time to 30 min, only 46 wt% Au nanoparticles were dissolved in Au@PPy/Fe_3O_4 hollow capsules. For Fe_3O_4 nanoparticles, in the same condition, the bare Fe_3O_4 nanoparticles were quickly dissolved within 30 min. In contrast, the weight percentage of the dissolved Fe_3O_4 in Au@PPy/Fe_3O_4 hollow capsules was only 35 wt%. Based on the data obtained from above two experiments, we could conclude once the metal nanoparticles were anchored on the support surface, two major problems they faced were falling off and deactivation due to erosion by solution. Wrapping nanoparticles in the hollow capsule shells could well resolve these disadvantages at the same time. Compared Au@PPy/Fe_3O_4 hollow capsules with precursor PS/Au composites, the catalytic activity of former was lower owing to the poor reactant contacting; however, the stability of former was much higher than latter. Moreover, Au@PPy/Fe_3O_4 hollow capsules could be quickly recycled due to incorporation of magnetic nanoparticles; therefore, they had better reusability. In our system, the PPy/Fe_3O_4 shell not only served as traditional support to load catalysts, but also separated nanoparticles from contacting with each other, restricted nanoparticles from escaping to exterior and protected nanoparticles from being corroded by solution. Because of these merits, in comparison with anchoring metal nanoparticles on the support surface, wrapping metal nanoparticles in polymer shell endowed catalysts much higher stability.

Conclusions

In summary, we have introduced a simple way to prepare Au@PPy/Fe_3O_4 hollow capsules. PS/Au composites were firstly synthesized through electrostatic interaction between sodium citrate stabilized Au nanoparticles and PDDA modified PS nanospheres; and then PPy/Fe_3O_4 shell was covered on the surface of PS/Au composites in one-step. After soaked in THF solution, PS cores were removed and the resulting Au@PPy/Fe_3O_4 hollow capsules were synthesized. In preparation procedure, $FeCl_3 \cdot 6H_2O$ played important roles, as it acted as both initiator for pyrrole monomer and source of Fe_3O_4 nanoparticles, simultaneously. Because the $FeCl_3 \cdot 6H_2O$ were excess in system, the magnetic property of catalysts was depended on the dosage of $FeCl_2 \cdot 4H_2O$. When the amount of $FeCl_2 \cdot 4H_2O$ was 10, 30 and 50 mg in system, the saturation magnetization value of catalysts was 27.3, 34.7 and 38.5 emu/g, respectively. Au@PPy/Fe_3O_4 hollow capsules exhibited excellent catalytic activity towards the reduction of MB dye solution with $NaBH_4$ as reducing agent. The reaction rate constant was 0.266 min^{-1}, which was much higher than their rate constant in absence of catalysts (3.68×10^{-2} h^{-1}). Due to incorporation of Fe_3O_4 nanoparticles, the catalysts could be easily separated from reaction solution by external magnetic field, and they exhibited good reusability. No significant decrease

in catalytic activity of Au@PPy/Fe_3O_4 hollow capsules was detected, even after the catalytic experiments were repeated 5 times. Further study showed the reaction rate constant in each cycle gradually reduced; however, the gradual reduction was mainly caused by unavoidable loss of catalysts during the separation and rinsing. Besides catalytic activity and reusability, the high stability was another merit for catalysts. Owing to the protection of PPy chain, the stability of Au and Fe_3O_4 nanoparticles was greatly improved. In both ultrasonic treatment and aqua regia solution etching test, the stability of Au@PPy/Fe_3O_4 hollow capsules was superior to that of precursor PS/Au composites. Since Au@PPy/Fe_3O_4 hollow capsules showed excellent catalytic activity, good reusability and high stability, together with a simple preparation procedure, they were potentially applicable in the treatment of industrial waste water.

Acknowledgements

This work was supported by the National Nature Science Foundation of China (Grant no. 51273051, 21174033, 21204015), Open Project of State Key Laboratory of Supramolecular Structure and Materials (No.sklssm 201410), Heilongjiang Postdoctoral Science-Research Foundation (No. LBH-Q13057) and the Specialized Research Joint Found for the Doctoral Program of Higher Education of China (No.20122301120003).

Reference

1. W. P. To, K. T. Chan, G. S. M. Tong, C. S. Ma, W. M. Kwok, X. G. Guan, K. H. Low and C. M. Che, *Angew. Chem. Int. Ed.*, 2013, **52**, 6648-6652.
2. S. Roy, G. Palui and A. Banerjee, *Nanoscale*, 2012, **4**, 2734-2740.
3. E. C. Dreaden, A. M. Alkilany, X. H. Huang, C. J. Murphy and M. A. El-Sayed, *Chem. Soc. Rev.*, 2012, **41**, 2740-2779.
4. B. N. Zope, D. D. Hibbitts, M. Neurock and R. J. Davis, *Science*, 2010, **330**, 74-78.
5. M. Clement, H. Menard and P. A. Rowntree, *Langmuir*, 2008, **24**, 8045-8049.
6. J. Han, L. Wang and R. Guo, *J. Mater. Chem.*, 2012, **22**, 5932-5935.
7. L. R. Kong, X. F. Lu, X. J. Bian, W. J. Zhang and C. Wang, *ACS Appl. Mater. Interface*, 2011, **3**, 35-42.
8. J. Tian, L. Yuan, M. M. Zhang, F. Zheng, Q. Q. Xiong and H. Y. Zhao, *Langmuir*, 2012, **28**, 9365-9371.
9. T. J. Yao, T. Y. Cui, X. Fang, J. Yu, F. Cui and J. Wu, *Chem. Eng. J.*, 2013, **225**, 230-236.
10. Y. J. Li, X. F. Li, Y. L. Li, H. B. Liu, S. Wang, H. Y. Gan, J. B. Li, N. Wang, X. R. He and D. B. Zhu, *Angew. Chem. Int. Ed.*, 2006, **45**, 3639-3643.
11. M. Graeser, E. Pippel, A. Greiner and J. H. Wendorff, *Macromolecules*, 2007, **40**, 6032-6039.
12. F. Wen, W. Q. Zhang, G. W. Wei, Y. Wang, J. Z. Zhang, M. C. Zhang and L. Q. Shi, *Chem. Mater.*, 2008, **20**, 2144-2150.
13. Q. Zhang, T. R. Zhang, J. P. Ge and Y. D. Yin, *Nano Lett.*, 2008, **8**, 2867-2871.
14. V. Polshettiwar, R. Luque, A. Fihri, H. B. Zhu, M. Bouhrara and J. M. Basset, *Chem. Rev.*, 2011, **111**, 3036-3075.
15. K. Katagiri, M. Nakamura and K. Koumoto, *ACS Appl. Mater. Interface*, 2010, **2**, 768-773.
16. W. T. Hu, B. C. Liu, Q. Wang, Y. Liu, Y. X. Liu, P. Jing, S. L. Yu, L. X. Liu and J. Zhang, *Chem. Commun.*, 2013, **49**, 7596-7598
17. J. P. Ge, Q. Zhang, T. R. Zhang and Y. D. Yin, *Angew. Chem. Int. Ed.*, 2008, **47**, 8924-8928.
18. A. B. Fuertes, T. Valdés-Solís, M. Sevilla and P. Tartaj, *J. Phys. Chem. C*, 2008, **112**, 3648-3654.
19. M. Kim, K. Sohn, H. B. Na and T. Hyeon, *Nano Lett.*, 2002, **2**, 1383-1387.
20. W. S. Choi, H. M. Yang, H. Y. Koo, H. Lee, Y. B. Lee, T. S. Bae and I. C. Jeon, *Adv. Funct. Mater.*, 2010, **20**, 820-825.
21. T. J. Yao, T. Y. Cui, X. Fang, J. Yu, F. Cui and Jie Wu, *Chem. Eng. J.*, 2013, **225**, 230-236.
22. S. H. Xuan, Q. L. Fang, L. Y. Hao, W. Q. Jiang, X. L. Gong, Y. Hua, Z. Y. Chen, *J. Colloid Interf. Sci.*, 2007, **314**, 502-509.
23. J. M. Li, W. F. Ma, C. Wei, J. Guo, J. Hu and C. C. Wang, *J. Mater. Chem.*, 2011, **21**, 5992-5998.
24. M. Y. Zhu and G. W. Diao, *J. Phys. Chem. C*, 2011, **115**, 18923-18934.
25. Z. M. Zhang, J. Y. Deng, J. Y. Shen, M. X. Wan and Z. J. Chen, *Macromol. Rapid Commun.*, 2007, **28**, 585-590.
26. H. M. Xiao, W. D. Zhang, M. X. Wan and S. Y. Fu, *J. Polym. Sci. Part A: Polym. Chem.*, 2009, **47**, 4446-4453.
27. J. J. Xu, J. C. Hu, B. G. Quan and Z. X. Wei, *Macromol. Rapid Commun.*, 2009, **30**, 936-940.
28. J. Liu, Z. K. Sun, Y. H. Deng, Y. Zou, C. Y. Li, X. H. Guo, L. Q. Xiong, Y. Gao, F. Y, Li and D. Y. Zhao, *Angew. Chem. Int. Ed.*, 2009, **48**, 5875-5879.
29. S. R. Yun, G. O. Kim, C. W. Lee, N. J. Jo, Y. Kang and K. S. Ryu, *J. Nanomater.*, **2012**, 894539-894548.
30. Y. Y. Yin, M. Chen, S. X. Zhou and L. M. Wu, *J. Mater. Chem.*, 2012, **22**, 11245-11251.
31. Y. F. Zhu, E. Kockrick, T.Ikoma, N. Hanagata and S. Kaskel, *Chem. Mater.*, 2009, **21**, 2547-2553.
32. T. Fujii, F. M. F. de Groot, G. A. Sawatzky, F. C. Voogt, T. Hibma and K. Okada, *Phys. Rev. B*, 1999, **59**, 3195-3202.
33. Q. Han, Z. H. Liu, Y. Y. Xu, Z. Y. Chen, T. M. Wang and H. Zhang, *J. Phys. Chem. C*, 2007, **111**, 5034-5038.
34. L. Li, Y. Yang, J. Ding and J. M. Xue, *Chem. Mater.*, 2010, **22**, 3183-3191.
35. F. X. Redl, C. T Black, G. C. Papaefthymiou, R. L. Sandstrom, M. Yin, H. Zeng, C. B. Murray, S. P. O' Brien, *J. Am. Chem. Soc.*, 2004, **126**, 14583-14599.
36. Y. Tao, E. G. Ju, J. S. Ren and X. G. Qu, *Chem. Commun.*, 2014, **50**, 3030-3032.
37. D. K. Dumbre, P. N. Yadav, S. K. Bhargava and V. R. Choudhary, *J. Catal.*, 2013, **301**, 134-140.
38. T. Mitsudome and K. Kaneda, *Green Chem.*, 2013, **15**, 2636-2654.
39. S. K. Ghosh, S. Kundu, M. Mandal and T. Pal, *Langmuir*, 2002, **18**, 8756-8760.
40. Y. H. Zhu, J. H. Shen, K. F. Zhou, C. Chen, X. L. Yang and C. Z. Li, *J. Phys. Chem. C*, 2011, **115**, 1614-1619.
41. E. Lam, S. Hrapovic, E. Majid, J. H. Chong and J. H. T. Luong, *Nanoscale*, 2012, **4**, 997-1002.
42. Y. Y. Yin, M. Chen, S. X. Zhou and L. M. Wu, *J. Mater. Chem.*, 2012, **22**, 11245-11251.
43. W. T. Hu, B. C. Liu, Q. Wang, Y. Liu, Y. X. Liu, P. Jing, S. L. Yu, L. X. Liu and J. Zhang, *Chem. Commun.*, 2013, **49**, 7596-7598.